ISA Transactions xxx (2018) 1–9

Contents lists available at ScienceDirect

ISA Transactions

journal homepage: www.elsevier.com/locate/isatrans

Research article

Grey Wolf based control for speed ripple reduction at low speed operation of PMSM drives☆

Ali Djerioui [a,b,*], Azeddine Houari [b], Mourad Ait-Ahmed [b], Mohamed-Fouad Benkhoris [b], Aissa Chouder [a], Mohamed Machmoum [b]

[a] LGE Laboratory, University of Msila, Algeria
[b] IREENA Laboratory, University of Nantes, Saint-Nazaire, France

ARTICLE INFO

Article history:
Received 25 July 2017
Revised 16 December 2017
Accepted 1 January 2018
Available online XXX

Keywords:
Speed control
Grey Wolf algorithm
Low speed operation
Permanent Magnet Synchronous Machine (PMSM)

ABSTRACT

Speed ripple at low speed-high torque operation of Permanent Magnet Synchronous Machine (PMSM) drives is considered as one of the major issues to be treated. The presented work proposes an efficient PMSM speed controller based on Grey Wolf (GW) algorithm to ensure a high-performance control for speed ripple reduction at low speed operation. The main idea of the proposed control algorithm is to propose a specific objective function in order to incorporate the advantage of fast optimization process of the GW optimizer. The role of GW optimizer is to find the optimal input controls that satisfy the speed tracking requirements. The synthesis methodology of the proposed control algorithm is detailed and the feasibility and performances of the proposed speed controller is confirmed by simulation and experimental results. The GW algorithm is a model-free controller and the parameters of its objective function are easy to be tuned. The GW controller is compared to PI one on real test bench. Then, the superiority of the first algorithm is highlighted.

1. Introduction

Permanent Magnet Synchronous Motors are employed in various applications such as electrical or hybrid electrical vehicles, elevator drives, and generically variable speed applications, where smooth speed regulation is required. The study of speed control of PMSM in normal mode with or without mechanical sensors is still in progress [1–3]. However, at critical operation conditions, low speed-high torque operation, low-frequency torque ripples occur and generate a severe speed ripples [4–6]. Commonly, a speed lower than 20% of the nominal speed can be considered a low speeds and a torque higher than 80% of the nominal torque can be considered as a high torque. The generated ripples can be seriously harmful due to temperature rise in the stator windings and fatigue phenomena in the shaft material, which leads to a significant reduction in the lifetime of the overall system.

Several control approaches to minimize the low-frequency torque ripples in PMSM have been reported in the literature [7–14]. For example, in Ref. [7], the disturbance frequency arising from current sensor offsets is embedded in the design of a model predictive based controller (MPC) to minimize the torque ripple. Also, in Ref. [8] the measured offsets and presence of unequal sensor gains, which are possible sources of unbalanced phase currents, are compensated by a phase current reconstruction strategy. In Ref. [9], an improved torque predictive control (TPC) is proposed to reduce the torque ripple and improve the system dynamics. The main idea was to include both torque and stator-flux errors information in the control algorithm calculation. In Ref. [10], the effect of unbalanced stator resistances on the torque ripple is investigated. Then, it was shown that the estimated values of these resistances can be used to compensate the high-frequency components of the torque ripple. In Ref. [11], the proposed torque ripple reduction is based on instantaneous torque estimation with a rigorous analytical model that takes spatial harmonics into account. The work presented in Ref. [15] calculates the best current reference which minimizes the torque oscillation by the use of an algorithm based on ANN (Artificial Neural Networks). Other interesting compensating solutions can be found in the literature such as iterative current harmonics elimination and predictive sequential switching control techniques that integrate the inverter dynamic in the

☆ Fully documented templates are available in the elsarticle package on CTAN.

* Corresponding author. LGE Laboratory, University of Msila, Algeria.
E-mail address: Alidjerioui@yahoo.fr (A. Djerioui).

https://doi.org/10.1016/j.isatra.2018.01.012
0019-0578/

control algorithm, which is respectively reported in Refs. [16] and [17].

The classical solution for the reduction of torque ripple at low speeds is the use of current harmonic injection techniques [4,18,19]. For this, an additional algorithm is added to modify the reference current or directly the control voltage in order to reduce the speed ripple. The added algorithms are commonly based on disturbance observer approaches that need the knowledge of the torque ripples models (first harmonic (offset), flux harmonics, cogging torque.), where the disturbance is estimated by an observer and then compensated by subtracting it from the control signal. Even if these algorithms are efficient in steady state, their effect is negative in case of external perturbation (variable speed applications) because the algorithm tries to compensate the perturbation. In other approaches, as resonant controller [20] and embedded MPC control [7], the undesired frequency(ies) is (are) directly integrated in the controller design. In such controllers, if the undesired frequency(ies) changes due the operation condition of the drive (parametric variation, unknown perturbation …), the rejection of this new undesired frequency is not efficient because this(these) frequency(ies) is(are) not considered during the synthesis step. To ensure high performance control of PMSM drives at low speed operation, the present paper aims to present a free-model controller based on a recent optimization method. The main objective is to ensure speed tracking tasks with smooth evolution at low speed-high torque operation. The proposed optimization speed-controller is based on Grey Wolf algorithm, which is a new member of meta-heuristic algorithms proposed by Mirjalili in 2014 [21]. The philosophy of this optimization algorithm is inspired from the social behavior of grey wolves when they attack a prey. This algorithm moves the wolves group toward prey by updating location vector, which is an average of best locations of the group. It presents several advantages in terms of low computing complexity, high solution accuracy, convergence independence of initial conditions and its ability to deal with local minima. In this subject, a comparative study based on twenty nine test [21] with Particle Swarm Optimization (PSO), Gravitational Search Algorithm (GSA), Differential Evolution (DE), Evolutionary Programming (EP), and Evolution strategy (ES) has shown that GW algorithm is highly competitive in terms of local optima avoidance and convergence to the global optimum. In other comparative study [22], it was shown that GW optimization algorithm exhibits attracting features like robustness and fast convergence with a reduced number of search parameters. These proprieties are particularly important from the point of view of real time implementation. The aforementioned advantages are also reflected in various recent research works [23,24]. For example, in Ref. [23], GW is applied to find optimal sizing of a micro-grid. This is done by solving the cost minimization problem of the system under various constraints, such as the storage capacity and the load demand satisfaction. In Ref. [22], GW is used to the design of an MPPT controller working under normal and abnormal modes like shading conditions. In Refs. [24] and [25], the GW optimization algorithm is used for an optimal tuning of fuzzy controllers with a reduced process small time constant sensitivity.

In this paper, the use of a speed-controller based on the GW algorithm is motivated by the usefulness of GW approach for locating the minimum objective function with attracting proprieties like fast convergence and few adjustment parameters without needing to know the system parameters. The key idea is to incorporate the benefit of the fast optimization process of the GW optimizer in real-time working conditions in order to find the optimal trajectory of the input controls. The resulting control input should secures the desired speed tracking tasks with a reduced ripple at low speed-high torque working conditions. In addition, a comparison with a fairly known control method is performed to highlight the effectiveness of the proposed control method especially in terms of speed ripple reduction at low speed.

The synthesis method of the proposed control algorithm neither requires the introduction of a predefined frequency(ies) to be rejected nor additional observers. The desired performances (speed tracking and speed ripple reduction) are achieved thanks to the proposed objective function where both speed and current are minimized in a one-loop structured controller. The algorithm parameters are selected to minimize the speed ripples at low speed by generating adapted current profiles.

This paper is organized as follows. In section 2 and 3, descriptions of the studied system and one of the principal speed ripple sources in PMSM drives are respectively presented. Section 4 introduces the proposed GW speed-controller design methodology. Sections 5 and 6 present simulation and experimental results and discuss the effectiveness of the proposed control approach. Finally, section 7 summarizes the major contributions of this work.

2. System description

The topology of the studied system with the proposed GW-controller is depicted in Fig. 1. The drive is composed of a DC power supply, a three phase inverter and PMSM with smooth poles. The GW based speed-controller is developed in a one-loop structure. The electrical model of a smooth poles PMSM expressed in the synchronous Park frame is:

$$\boldsymbol{u_s} = R_s \boldsymbol{i_s} + \dot{\boldsymbol{\Psi}}_{\mathbf{s}} + \omega_e \begin{bmatrix} 0 & -1 \\ 1 & 0 \end{bmatrix} \boldsymbol{\Psi_s} \tag{1}$$

where $\boldsymbol{u_s} = [v_d\ v_q]^T$ is the stator voltage vector, $\boldsymbol{i_s} = [i_d\ i_q]^T$ is the stator current vector, $\boldsymbol{\Psi_s} = [\Psi_d\ \Psi_q]^T$ is the stator flux vector, R_s is the stator per-phase resistance, $\omega_e = p\,\Omega$ is the rotor electrical speed, p is the number of the pole pairs, Ω the mechanical angular speed of the rotor. The stator flux can be formulated as follows:

$$\boldsymbol{\Psi_s} = L_s i_s + \boldsymbol{\Psi_{pm}} \tag{2}$$

where $\Psi_{pm} = [\Psi_{pm}\ 0]^T$ is the magnet's flux and L_s is the stator inductance.

The motion equation is expressed as follows:

$$\dot{\Omega} = \frac{1}{J}(T_e - T_L - F\Omega) \tag{3}$$

In the above equation T_L is the load torque, F is the frictional coefficient and J is the moment of inertia. The electromagnetic torque equation is given by:

$$T_e = p\Psi_{pm} i_q \tag{4}$$

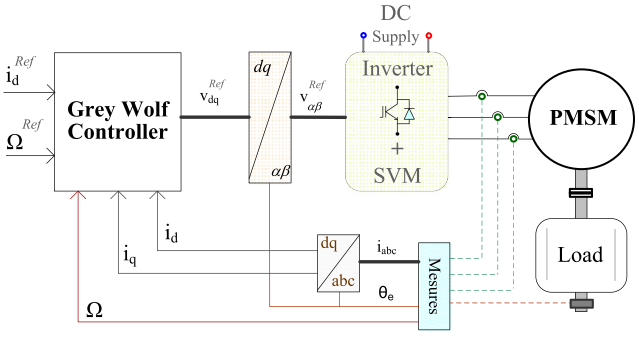

Fig. 1. Schematic of the PMSM speed regulation system based on GW controller.

3. Effect of back electromotive force on speed harmonics

Harmonics in back electromotive force (BEMF) can cause torque ripple. For example, if the phase currents of the stator are sinusoidal and the BEMF has harmonics 5 and 7 (the most predominant harmonics in a three-phase machine PMSM), then harmonic 6 that will appear on the torque.

Demonstration:

As the phase currents are sinusoidal, their expressions are:

$$\begin{cases} i_a = I\sin(\omega_e t) \\ i_b = I\sin\left(\omega_e t - \dfrac{2\pi}{3}\right) \\ i_c = I\sin\left(\omega_e t + \dfrac{2\pi}{3}\right) \end{cases} \tag{5}$$

The expressions of the BEMF in presence of harmonics 5 and 7 are:

$$\begin{cases} e_a = E_1\sin(\omega_e t) + E_5\sin(5\omega_e t) + E_7\sin(7\omega_e t) \\ e_b = E_1\sin\left(\omega_e t - \dfrac{2\pi}{3}\right) + E_5\sin\left(5\omega_e t - \dfrac{10\pi}{3}\right) + E_7\sin\left(7\omega_e t - \dfrac{14\pi}{3}\right) \\ e_c = E_1\sin\left(\omega_e t + \dfrac{2\pi}{3}\right) + E_5\sin\left(5\omega_e t + \dfrac{10\pi}{3}\right) + E_7\sin\left(7\omega_e t + \dfrac{14\pi}{3}\right) \end{cases} \tag{6}$$

The torque can be computed as:

$$T_e = \frac{P}{\Omega} = \frac{e_a i_a + e_b i_b + e_c i_c}{\Omega} \tag{7}$$

Then, the expression of the torque is:

$$T_e = \frac{3}{2\Omega}E_1 I - \frac{3}{2\Omega}\left(E_5 - E_7\right) I\cos\left(6\omega_e t\right) \tag{8}$$

To investigate the harmonic content in the BEMF, the test machine in this paper is coupled as a generator and conducted at low speed (100 rpm) under no load. Fig. 2 reports the time and frequency domains of the resulted back electromotive force (BEMF). The harmonic spectra illustrates the presence of low harmonic orders mainly caused by the coupling motor, and it can be seen that the most predominant harmonics are 5th and 7th. These harmonic contents can be considered as the principal source of the speed ripple in low speed operation.

According to (3), as it's a linear differential equation, the motor speed has the same harmonics (6 order harmonics) as the torque produced by the PMSM. It can be noted that when considering the other principal harmonic contents in the BEMF like: 11, 13, 17, 19, multiples of 6th harmonic appear in the speed.

4. Grey Wolf based speed-controller

This section presents the design methodology of the proposed GW speed-controller. The global control scheme of the PMSM drive is given in Fig. 1. Grey Wolf is a new member of swarm intelligence-based optimization algorithms, introduced in 2014 by Mirjalili [21]. The philosophy of this technique is inspired by the social behavior of grey wolves when they attack a prey. In a pack, the grey wolves have a very strict social dominant hierarchy where they are classified from the highest to the lowest hierarchy ranks called, alpha, beta, delta, and then the other hunters respectively. The complete theory of the Grey Wolf theory can be found in Ref. [21].

To formulate the PMSM control problem in accordance with the GW theory, three steps are to be defined: objective function formulation and evaluation, candidate input control calculation, and finally reference control selection.

4.1. Candidate objective function

The proposed objective function is inspired by the standard way of controlling PMSM electrical drives, i.e. vector control. Commonly, the conventional scheme is based on cascaded PI loops; i.e. an outer speed loop and an inner current loop. As usual in PMSM control, the d-axis current reference i_d^{ref} is fixed to zero and the quadratic current reference i_q^{ref} which presents the main electromagnetic torque is deduced directly from the speed outer loop. Contrary to classical approaches where the speed control is constructed within two loops, herein, the control problem is a MIMO one and it is formulated within one loop structure. The candidate objective function may summarize the global control objective: speed tracking tasks with smooth waveform at low speed operation. The proposed objective function **G** is defined as follows:

$$\mathbf{G[k]} = \left[\begin{array}{cc|ccc} K_1 & K_2T_s & 0 & 0 & 0 \\ --- & --- & ------- & -- & -- \\ 0 & 0 & K_3 + K_5T_s & K_5 & K_4 \end{array}\right]\boldsymbol{\sigma[k]} \tag{9}$$

where k is the current iteration, and $\mathbf{G[k]} = [G_d[k]\ G_q[k]]^T$ is the objective vector. The first objective function denoted $G_d[k]$ is characterized by the d-axis current $i_d[k]$ and the d-axis control input $u_d[k]$. The second objective function denoted $G_q[k]$ is characterized by the q-axis current $i_q[k]$, the speed $\Omega[k]$ and the q-axis control input $u_q[k]$. The minimization of this function is mainly related to the speed ripple amplitude. $\boldsymbol{\sigma}[k] = [\boldsymbol{\sigma_d}[\boldsymbol{k}], \boldsymbol{\sigma_q}[\boldsymbol{k}]]^T$, with $\boldsymbol{\sigma_d}[\boldsymbol{k}] = [i_d^{ref}[k] - i_d[k],\ i_d^{ref}[k-1] - i_d[k-1]]$, and $\boldsymbol{\sigma_q} = [\Omega^{ref}[k] - \Omega[k],\ \Omega^{ref}[k-1] - \Omega[k-1],\ i_q[k]]$. Parameters K_1, K_2, K_3, K_4, K_5 are con-

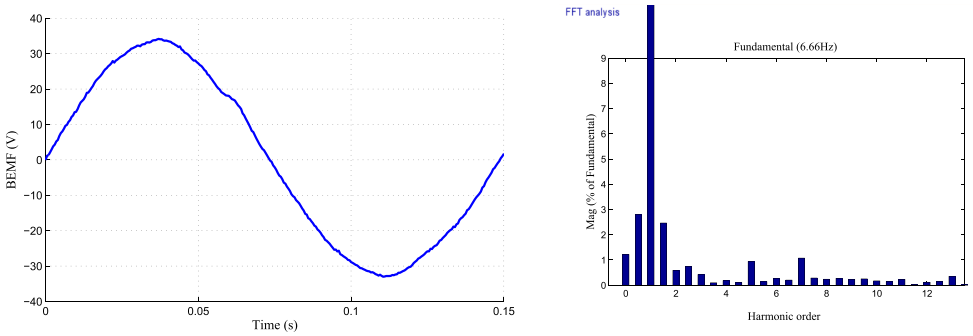

(a) (b)

Fig. 2. The BEMF of the PMSM working as a generator at 100 rpm speed and under no load: (a) phase (*a*) voltage, (b) harmonic components of phase voltage (a).

Please cite this article in press as: Djerioui A, et al. Grey Wolf based control for speed ripple reduction at low speed operation of PMSM drives, ISA Transactions (2018), https://doi.org/10.1016/j.isatra.2018.01.012

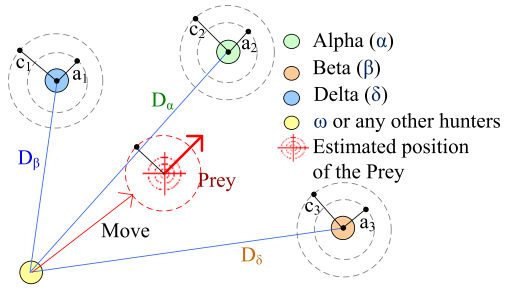

Fig. 3. Principle of grey wolves hunting [21].

stant gains whose design is presented in the simulation part. T_s is the sample time.

4.2. Optimal hunting distance calculation

The algorithm mechanism searches three best solutions among the global possible hunting solutions and then calculates the attacking candidate input control (inverter voltages). The mechanism of the hunting is depicted in Fig. 3. The three best solutions obtained can be formulated as follows:

$$\left\| \begin{bmatrix} D_{x\alpha}[k] \\ D_{x\beta}[k] \\ D_{x\gamma}[k] \end{bmatrix} \right\| = \left\| \begin{bmatrix} C_{x1} & 0 & 0 \\ 0 & C_{x2} & 0 \\ 0 & 0 & C_{x3} \end{bmatrix} \begin{bmatrix} v_{x\alpha}[k] \\ v_{x\beta}[k] \\ v_{x\gamma}[k] \end{bmatrix} - \begin{bmatrix} G_x[k] \\ G_x[k] \\ G_x[k] \end{bmatrix} \right\| \tag{10}$$

where $C_{xi} = 2a_{xi}r_{xi}$, $x = \{d, q\}$, r_{xi} are random vectors whose values are within [0, 1], a_{xi} are linearly decreased from 2 to 0 over. The optimal distance vector $[D_{x\alpha}[k]\ D_{x\beta}[k]\ D_{x\gamma}[k]]^T$, is then used to formulate intermediate input control variables $[v_{x\alpha}[k+1]\ v_{x\beta}[k+1]\ v_{x\gamma}[k+1]]^T$ as defined in (Eq. (11)).

$$\begin{bmatrix} v_{x1}[k+1] \\ v_{x2}[k+1] \\ v_{x3}[k+1] \end{bmatrix} = \begin{bmatrix} v_{x\alpha}[k] \\ v_{x\beta}[k] \\ v_{x\gamma}[k] \end{bmatrix} - \begin{bmatrix} A_{x1} & 0 & 0 \\ 0 & A_{x2} & 0 \\ 0 & 0 & A_{x3} \end{bmatrix} \begin{bmatrix} D_{x\alpha}[k] \\ D_{x\beta}[k] \\ D_{x\gamma}[k] \end{bmatrix} \tag{11}$$

where $A_{xi} = 2a_{xi}\ r_{xi} - a_{xi}$, $i \in \{1,2,3\}$, and $x = \{d, q\}$.

Finally, by the use of the predefined intermediate control variables, the candidate dq-input control (inverter voltages) are calculated by:

$$v_x^{ref}[k+1] = \sum_{i=1}^{i=n} \frac{v_{xi}[k+1]}{3} \tag{12}$$

4.3. Reference control selection

The final design step consists in the evaluation of the established control solutions in step 2. Herein, the established control solutions are parameterized by their specified distance $|A_{xi}|$. Therefore, the d-q axis input control voltages are selected as follow:

$$\begin{cases} u_x^{ref} = v_x^{ref}[k+1] & if(|A_{xi}| < 1) \\ u_x^{ref} = v_x^{ref}[k] & if(|A_{xi}| > 1) \end{cases} \tag{13}$$

where $x = \{d, q\}$, $v_x^{ref}[k]$ is the actual input control, $v_x^{ref}[k+1]$ is the future input control, and u_x^{ref} is the input control. The candidate input control established in step 2, and its specified distance $|A_{xi}|$ are evaluated ($|A_{xi}|$ compared to 1) in order to predict the future input control.

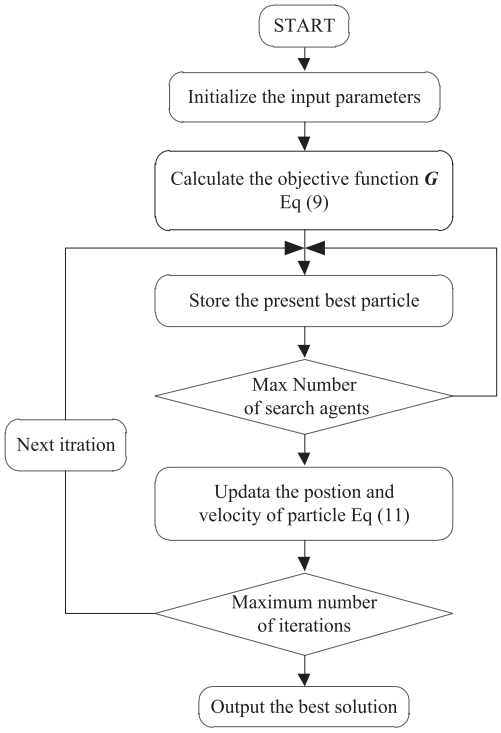

Fig. 4. Flowchart of the proposed GW algorithm.

4.4. Flowchart of the GW algorithm

The flowchart of the proposed GW algorithm is shown in Fig. 4. Adding to the design methodology, decrypted previously, the algorithm must be initialized. In this phase, the parameters must be set by including the maximum cycle number search agents, the sampling time, and the distance variables $|A_{xi}|$ and $|C_{xi}|$. Then, a randomly distributed initial reference voltage is generated. To highlight the importance of the iteration number in the control effectiveness, especially in the point of view on-line optimization, supporting simulation results are given in the following section.

5. Simulation results

In order to investigate how the GW algorithm iteration number influences the early stage convergence and how the objective function parameters are selected to reduce speed ripples, simulation tests have been carried out using MATLAB/Simulink. The PMSM motor parameters are listed in Table 1, (see APPENDIX).

5.1. Algorithm convergence

Fig. 5 (a) and (b) illustrate the initial position of the q-axis intermediate input control variables ($v_{q1}^{ref}, v_{q2}^{ref}, v_{q3}^{ref}$) at the early stage different iteration numbers respectively: 3 and 30. It can be observed

Table 1
Performance indicators.

Control strategy	Peak overshoot (%)	$IAE = \int \|e\|\, dt$	$ISE = \int \|e\|^2 dt$	$ITAE = \int t\|e\|\, dt$
PI controller	15.5	6.1	22.46	6.791
Proposed controller	0	1.616	1.813	1.882

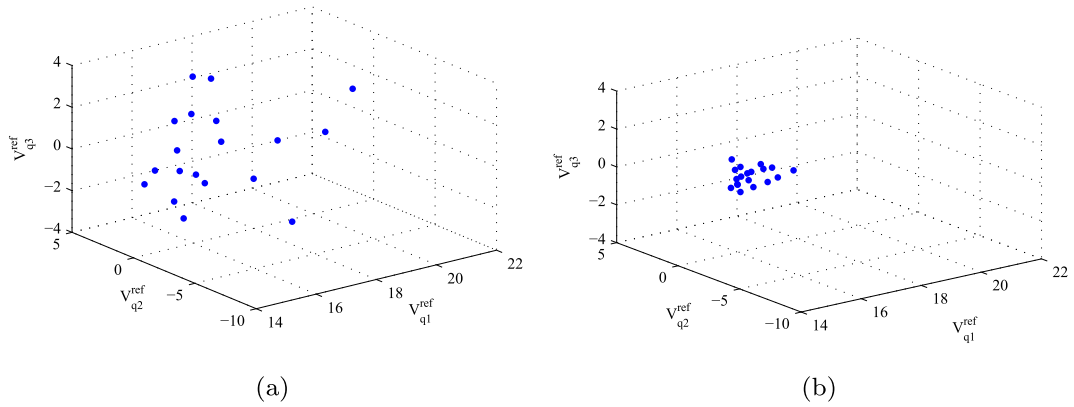

Fig. 5. Initial position of the q-axis intermediate input control variables at the early stage for: (a) 3 iterations; (b) 30 iterations.

that the particles are more and more attracted when the iteration number is increased. Fig. 6 confirms the overall trend of the solution convergence versus the iteration number. In this figure, the proposed convergence criterion presents the Root Mean Squared Error (RMSE) of the particules along the q-axis, calculated by:

$$RMSE = \sqrt{\sum_{k=1}^{n} \frac{\frac{1}{3}\sum_{i=1}^{3}(v_{qi}[k] - (v_q^{ref}))^2}{n}} \tag{14}$$

Considering this result, the iteration number is chosen equal to 20, which satisfies both convergence precision and minimizes time calculation regarding real time implementation.

5.2. Objective function parameters tuning

The second simulation test highlights the setting of the objective function parameters regarding speed ripple rate. In this test, the case of non-sinusoidal flux density distribution in the air gap of the PMSM that causes the 6th harmonic and its multiples is considered.

Also, low order harmonics caused by the coupling load are added. The test mechanism is described in Fig. 7. The parameters of the objective function are changed sequentially and the corresponding SRF values are calculated.

Fig. 8(a) illustrates the evolution of the speed ripple factor (SRF) versus the q-axis objective function parameters when the parameter K_5 is set to 0.01 and K_3 and K_4 are changed from 0 to 20. It can be seen that the SRF evolution is more sensitive to the change of K_4 and its values are minimized for K_4 greater than 5.

This gain is related to the q-axis current (Eq. (9)), which is the main component for the production of the torque in smooth poles PMSM. Therefore and as explained in section 3, the speed harmonics are mainly related to the torque harmonic content. Than, the reduction of the torque ripple lead to ensure smooth speed.

Fig. 8(b) illustrates the evolution of the SRF versus the d-axis objective function parameters when the parameter K_1 and K_2 are changed from 0 to 30. Herein, the SRF values are not affected by the change of K_1 and K_2, which means that the control objectives are well decoupled.

In other hand, gains K1 and K3 should be selected not very high to avoid big overshoots on transients conditions. Therefore, a trade-off must be done to choose the adequate values. In our case, the chosen values are: $K_1=4$, $K_2=15$, $K_3=0.2$, $K_4=10$, and $K_5=0.01$.

5.3. Performance illustration

To underline the performance of the proposed speed controller, comparison tests with a classical field oriented control method based on cascaded PI loops is considered. The current control loop calculates the control inputs:

$$\begin{aligned} v_d^{ref} &= K_{pi}(i_d^{ref} - i_d) + K_{ii}\int (i_d^{ref} - i_d)\overbrace{- w_e L_s i_q}^{Decoupling\ term} \\ v_q^{ref} &= K_{pi}(i_q^{ref} - i_q) + K_{ii}\int (i_q^{ref} - i_q) - w_e L_s i_d - w_e \Psi_{pm} \end{aligned} \tag{15}$$

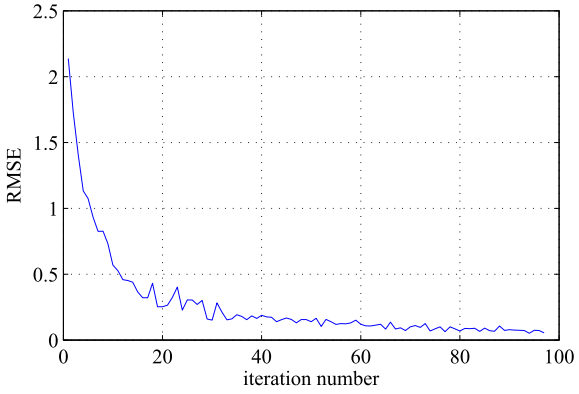

Fig. 6. Root Mean Squared Errors of the intermediate input control versus the iteration number.

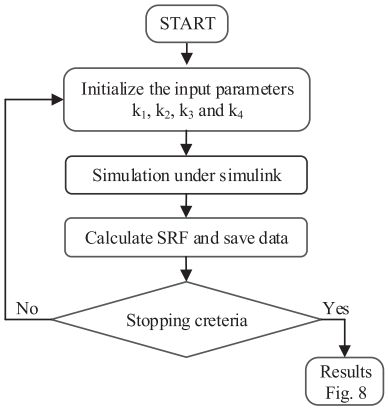

Fig. 7. Flowchart of the objective function parameters selection.

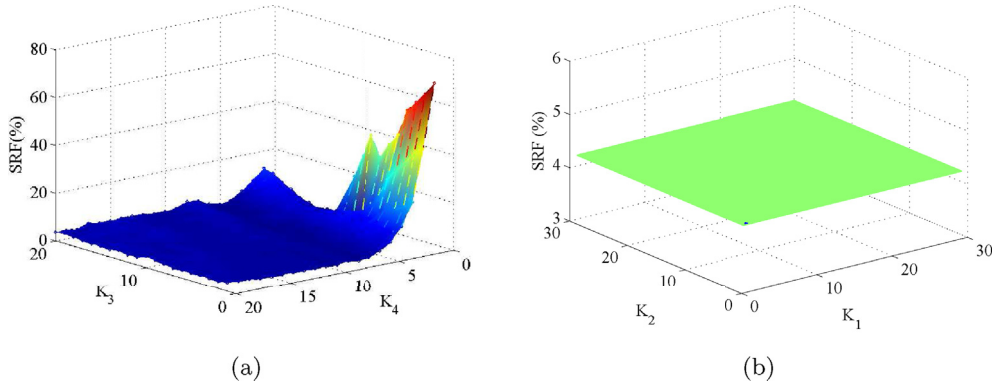

Fig. 8. Evolution of the speed ripple factor (SRF) versus the objective function parameters: (a) G_q parameters (K_3 and K_4); (b) G_d parameters (K_1 and K_2).

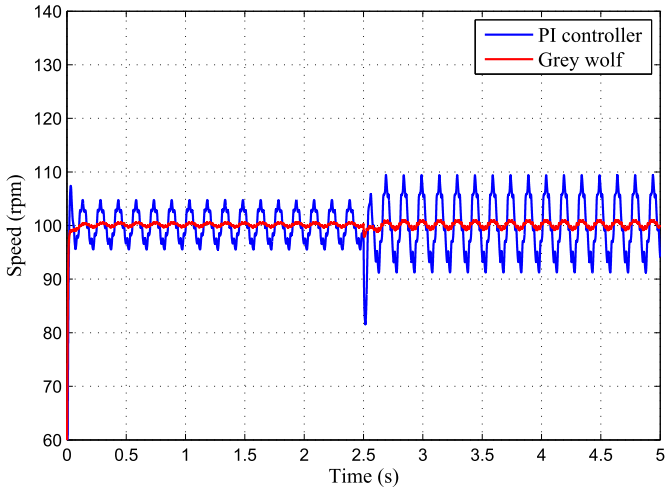

Fig. 9. Measured speeds for a classical PI controller and the proposed GW controller.

As usual in non-salient PMSM control, the d-axis current reference i_d^{ref} is fixed to zero while the quadratic current reference i_q^{ref} results from the outer speed control loop.

$$i_q^{ref} = K_{pw}(w_e^{ref} - w_e) + K_{iw}\int (w_e^{ref} - w_e) \tag{16}$$

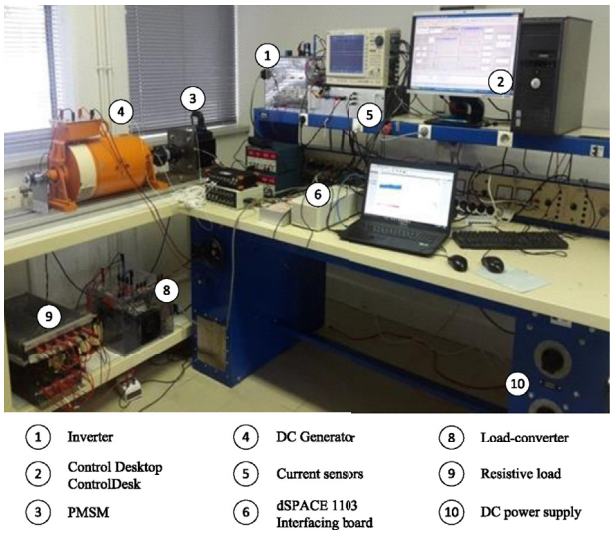

Fig. 10. Overview of the test bench.

5.3.1. PI synthesis method

The controller design is based on the pole-placement technique [4,26–29]. In terms of Laplace transform, the speed and currents closed-loop transfer functions are given by:

$$\frac{i_x}{i_x^{ref}} = \frac{(K_{pi}s + K_{ii})}{s^2 + \frac{(K_{pi}+R_s)}{L_s}s + \frac{K_{ii}}{L_s}} \tag{17}$$

$$\frac{\omega_e}{\omega_e^{ref}} = \frac{\frac{(K_{p\omega}s + K_{i\omega})(p^2\Psi_f)}{J}}{s^2 + \frac{K_{p\omega}p^2\Psi_f}{J}s + \frac{K_{i\omega}p^2\Psi_f}{J}} \tag{18}$$

where x = d,q.

It can be noted that the speed closed-loop transfer function (18) is obtained by considering an ideal current loop behavior and by neglecting the friction torque.

The controller gains (K_{pi}, K_{ii}, K_{pw} and K_{iw}) are selected by matching the denominator polynomial to the desired second order characteristic polynomial: $s^2 + 2\xi\omega_y s + \omega_y^2 = 0$, w_y denotes the controllers natural frequencies (y = c, ω: index c for current and ω for speed), The resulting control gains are $K_{pi} = (2\xi L_s\omega_c - R_s)$, $K_{ii} = L_s\omega_c^2$, $K_{p\omega} = (2\xi J\omega_\omega)/(p^2\Psi_f)$ and $K_i\omega = (J\omega_\omega^2)/(p^2\Psi_f)$.

The poles of the closed-loop control are characterized by the damping coefficients ξ and by the natural frequency ω_y:

$$P_{z1z2} = -\omega_y(\xi \pm \sqrt{(1-\xi^2)}) \tag{19}$$

The control objectives aim to ensure high speeds tracking performance (outer loop) and efficient disturbances rejection (inner loop). This leads to choose large values of the natural control frequencies (w_c and w_w). Otherwise, the natural frequency of the outer loop should be chosen sufficiently smaller (typically by ten times) than that of the inner loop to avoid interaction issues between the two loops. In addition, the inner loop natural frequency must be chosen sufficiently below the inverter switching frequency ($f_{sw} = 10$ kHz). In other hand, w_c must be greater than the current open-loop cut-off frequency ($R_s/L_s = 52\ rad/s$), while w_w must be greater than the speed open-loop cut-off frequency ($F/J = 1.15\ rad/s$). For our application, w_c and w_w are chosen equal to 1500 rad/s and 100 rad/s, respectively. Hence, the controllers gains are: $K_{pi} = 9.9308$, $K_{ii} = 10800$, $K_{p\omega} = 0.21375$ and $K_{i\omega} = 15.112$.

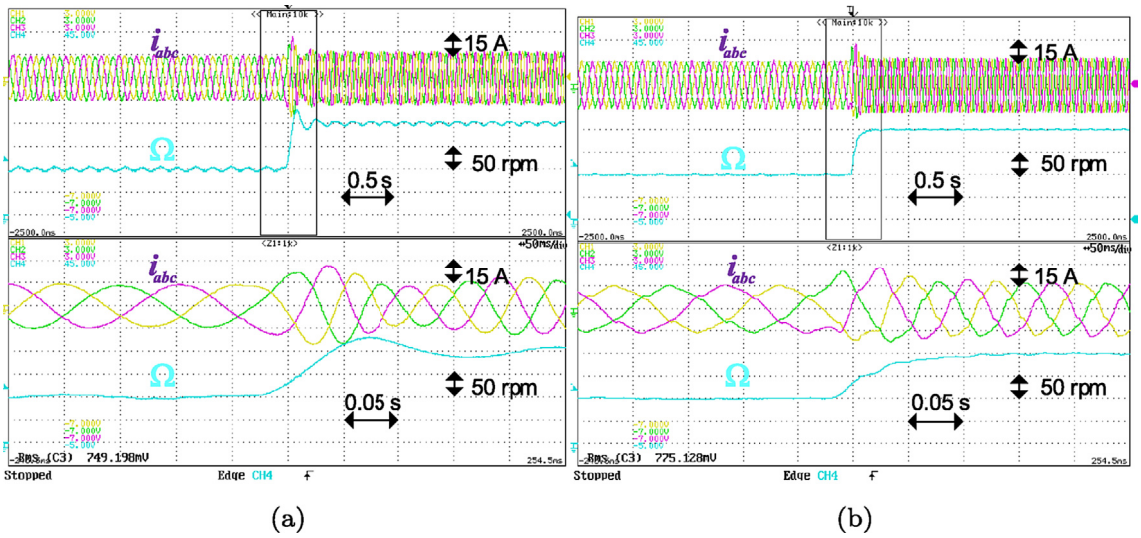

Fig. 11. Experimental plots: speed and abc current responses for speed change from 100 to 200 rpm under nominal-load with: (a) a classical PI controller, (b) the proposed controller.

5.3.2. Simulation analysis

Fig. 9 illustrates the measured speeds for a classical PI controller (blue color) and the proposed GW controller (red color). In this test the speed reference is fixed to 100 rpm. The load torque is changed from 14.2 to 28.4 Nm at t = 2.5 s. It can be noted that the proposed controller allows minimizing the oscillating speed at steady state and reduces significantly the speed drop when the disturbance occurs. Measured speed drop is around 3% with the GW controller and 18% with the classical PI controller.

6. Experimental results

In order to validate the system performance with the proposed control strategy, experiments are carried out. The picture of the experimental setup is shown in Fig. 10. The test bench consists of a PMSM and a DC generator load. The proposed PMSM control is implemented in a dSPACE DS1103 PPC.

Classical PI and the proposed GW speed-controller are tested when the speed reference changes from 100 to 200 rpm under a nominal load (28.4 Nm). In the case of a classical PI, Fig. 11(a), one can remark that the speed waveform presents oscillations when the stator currents waveforms are sinusoidal. When the proposed GW speed-controller is tested, Fig. 11(b), it can be noted that the speed waveform is more smoother than the one presented in Fig. 11(a). To ensure this speed oscillations reduction, the GW controller introduce harmonics in the stator currents profiles (Fig. 11(b)). In this subject, as mentioned in the introduction, classical methods add a compensator bloc that modifies currents profiles to achieve a smooth speed waveform. Also, it can be noted, with the GW controller that the motor velocity tracks its reference trajectory without overshoot.

To investigate the harmonic content of the speed at 100 rpm under nominal load torque, frequency spectrums are presented for both controllers in Fig. 12. These spectrums show the presence of specific harmonic orders, particularly the 1th, 2th, 6th and 12th harmonics. When the 6th and 12th harmonic components can be related to the non-sinusoidal flux density distribution in the air-gap, the lowest order harmonics are mainly introduced by the coupling mechanical load. Compared to the spectrum obtained with the PI controller, it can be seen that the specific harmonic amplitudes are significantly reduced with the use of the proposed controller.

Fig. 13(a) and (b) show the system behavior with a classical PI and the proposed GW speed-controller where the speed reference is kept constant (100 rpm) under load torque step from half nominal (14.2 Nm) to nominal torque (28.4 Nm). Likewise, speed oscillations are reduced with GW controller compared to the classical PI controller. Furthermore, the speed deviation is reduced with the GW controller when the load disturbance is applied. Indeed, the speed drop is around 10% with the GW controller and 25% with the classical PI controller.

In Table 1, different indicators are reported: peak overshoot, integral absolute error (IAE), integral of square error (ISE) and integral

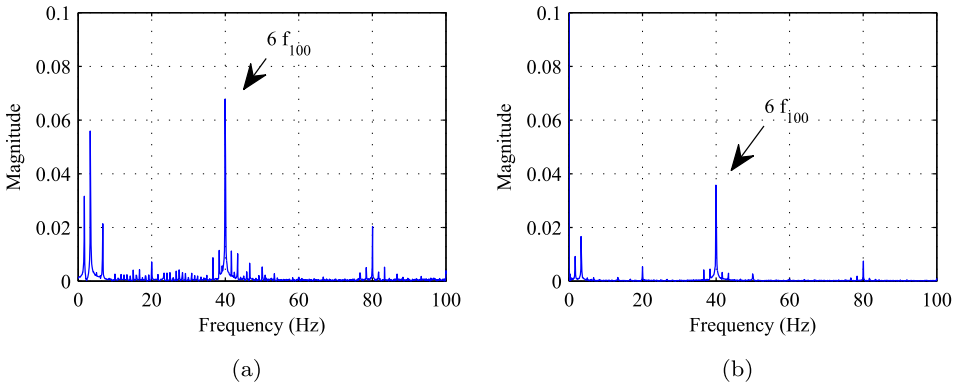

Fig. 12. Frequency spectrum of the speed at 100 rpm under nominal torque with: (a) a classical PI; (b) the proposed controller.

Please cite this article in press as: Djerioui A, et al. Grey Wolf based control for speed ripple reduction at low speed operation of PMSM drives, ISA Transactions (2018), https://doi.org/10.1016/j.isatra.2018.01.012

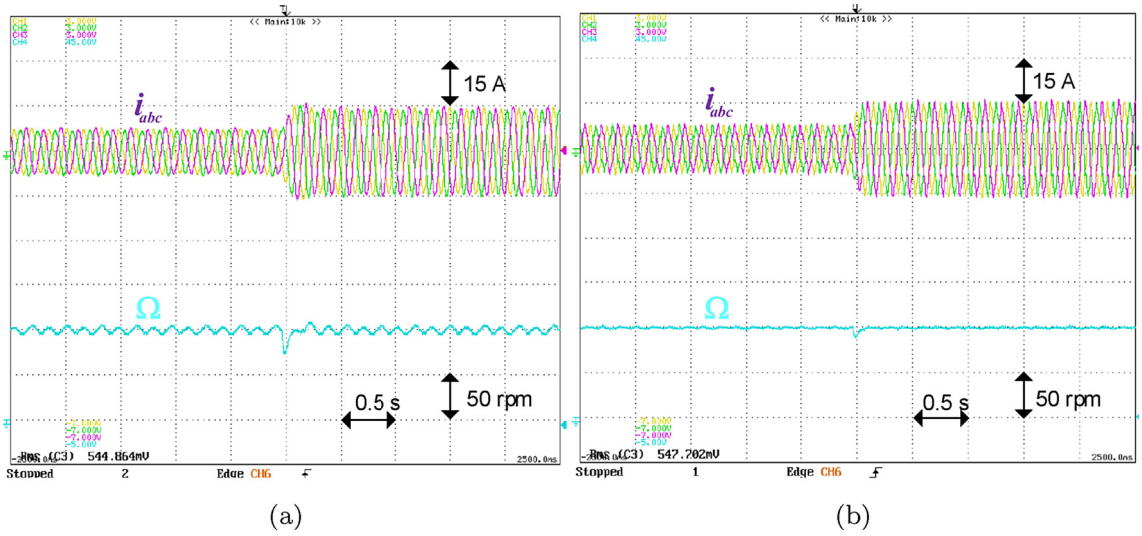

Fig. 13. Experimental plots: speed and abc current responses at 100 rpm speed under step load (14.2 Nm to 28.4 Nm) with: (a) a classical PI, (b) the proposed controller.

time absolute error (ITAE). As it can be appreciated, these indicators highlight the superiority of the proposed control algorithm.

7. Conclusion

This paper has proposed a GW algorithm for high performance control of PMSM drives. The proposed controller aims to ensure speed tracking tasks at low-speed high-torque while minimizing the ripples. The main idea of the proposed speed controller is to exploit the fast optimization process of the GW optimization algorithm in real time working conditions to find the optimal control inputs that ensure the desired speed tracking with a smooth speed time evolution. The design methodology of the GW based speed controller is detailed, and the influence of the objective function parameters in the torque ripple is analyzed in the simulation part. The real time implementation is performed under dSPACE 1103 control board and the obtained results verify the feasibility of the proposed approach. To underline, the improvement of the GW speed-controller a comparative student with a classical PI controller are provided.

As perspective, further comparisons with advanced control methods like intelligence-based algorithms (PSO, ANN …) are needed to provide better comprehension on the GW controller effectiveness under real time working conditions. The use of the GW optimization algorithm can be extended to solve speed or torque tracking tasks of others PMSM drives where low order harmonics are undesired and classical control algorithms are not effective.

Appendix

The system parameters are listed in Table 1.

Table 2
System Parameters.

PMSM Parameters	Value
Stator resistance	0.25 Ω
Stator inductance	4,8 mH
Number of the pole pairs	4
Magnet flux	0.32 Wb
Inertia	0,00774 kg m^2
Frictional coefficient	0,0089 Nm/s
Nominal speed	1500 rpm
Nominal torque	28.4 Nm

References

[1] Qiao W, Tang X, Zheng S, Xie Y, Song B. Adaptive two-degree-of-freedom PI for speed control of permanent magnet synchronous motor based on fractional order GPC. ISA Trans 2016;64:303–13. https://doi.org/10.1016/j.isatra.2016.06.008.

[2] Li L-B, Sun L-L, Zhang S-Z, Yang Q-Q. Speed tracking and synchronization of multiple motors using ring coupling control and adaptive sliding mode control. ISA Trans 2015;58:635–49. https://doi.org/10.1016/j.isatra.2015.07.010.

[3] Chen S, Luo Y, Pi Y. Letter to the Editor PMSM sensorless control with separate control strategies and smooth switch from low speed to high speed. ISA Trans 2015;58:650–8. https://doi.org/10.1016/j.isatra.2015.07.013.

[4] Houari A, Bouabdallah A, Djerioui A, Machmoum M, Auger F, Darkawi A, et al. An effective compensation technique for speed smoothness at low speed operation of PMSM drives. IEEE Trans Ind Appl 2017;PP(6):1–1. http://doi.org/10.1109/TIA.2017.2740388.

[5] Wu L-H, Liu Z-H, Li X-H. GPU-accelerated parallel Co-evolutionary algorithm for parameters identification and temperature monitoring in permanent magnet synchronous machines. IEEE Trans Ind Inf 2015;11:1220–30.

[6] Dong X, Shaoguang Z, Jingmeng L. Very-low speed control of PMSM based on EKF estimation with closed loop optimized parameters. ISA Trans 2013;52(4):835–43. https://doi.org/10.1016/j.isatra.2013.06.008.

[7] Chai S, Wang L, Rogers E. A cascade MPC control structure for a PMSM with speed ripple minimization. IEEE Trans Ind Electron 2013;60(8):2978–87. https://doi.org/10.1109/TIE.2012.2201432.

[8] Cho Y, Member S, Labella T, Member S. A three-phase current reconstruction strategy with online current offset compensation. IEEE Trans Ind Electron 2012;59(7):2924–33.

[9] Cho Y, Lee KB, Song JH, Lee YI. Torque-ripple minimization and fast dynamic scheme for torque predictive control of permanent-magnet synchronous motors. IEEE Trans Power Electron 2015;30(4):2182–90. https://doi.org/10.1109/TPEL.2014.2326192.

[10] Xu Y, Parspour N, Vollmer U. Torque ripple minimization using online estimation of the stator resistances with consideration of magnetic saturation. IEEE Trans Ind Electron 2014;61(9):5105–14. https://doi.org/10.1109/TIE.2013.2279378.

[11] Nakao N, Akatsu K. Suppressing pulsating torques: torque ripple control for synchronous motors. IEEE Ind Appl Mag 2014;20(6):33–44. https://doi.org/10.1109/MIAS.2013.2288383.

[12] Flieller D, Nguyen NK, Wira P, Sturtzer G, Ould D, Merckl J. A self-learning solution for torque ripple reduction for non-sinusoidal permanent magnet motor drives based on artificial neural networks. IEEE Trans Ind Electron 2014;61(2):1–12. https://doi.org/10.1109/TIE.2013.2257136.

[13] Luo Y, Chen Y, Pi Y. Cogging effect minimization in PMSM position servo system using dual high-order periodic adaptive learning compensation. ISA Trans 2010;49(4):479–88. https://doi.org/10.1016/j.isatra.2010.05.003.

[14] Xudong L, Chenghui Z, Ke L. Robust current control-based generalized predictive control with sliding mode disturbance compensation for PMSM drives. ISA Trans 2017;PP(4):1–9. https://doi.org/10.1016/j.isatra.2017.08.015.

[15] Pajchrowski T, Zawirski K, Member S, Nowopolski K. Neural speed controller trained online by means of modified RPROP algorithm. IEEE Trans Ind Inf 2015;11(2):560–8.

[16] Yuan L, Chen M-L, Shen J-Q, Xiao F. Current harmonics elimination control method for six-phase PM synchronous motor drives. ISA Trans 2015;59:443–9. https://doi.org/10.1016/j.isatra.2015.09.013.

Please cite this article in press as: Djerioui A, et al. Grey Wolf based control for speed ripple reduction at low speed operation of PMSM drives, ISA Transactions (2018), https://doi.org/10.1016/j.isatra.2015.09.013

[17] Jezernik K, Korelič J, Horvat R. PMSM sliding mode FPGA-based control for torque ripple reduction. IEEE Trans Power Electron 2013;28(7):3549–56. https://doi.org/10.1109/TPEL.2012.2222675.
[18] Mandra S, Galkowski K, Ascheman H. Robust guaranteed cost ILC with dynamic feedforward and disturbance compensation for accurate PMSM position control. Contr Eng Pract 2017;65(4):36–7.
[19] Mi T, Gaeta A, Formentini A, Pericle Z. An effective compensation technique for speed smoothness at low speed operation of PMSM drives. IEEE Trans Ind Appl 2017;PP(5):1–1. http://doi.org/10.1109/TIA.2017.2725824.
[20] Xia C, Ji B, Yan Y. Smooth speed control for low-speed synchronous motor using proportional-integral-resonant controller. IEEE Trans Ind Electron 2015;62(4):2123–34. https://doi.org/10.1109/TIE.2014.2354593.
[21] Mirjalili S, Mohammad S, Lewis A. Grey Wolf optimizer. Adv Eng Software 2014;69:46–61.
[22] Mohanty S, Subudhi B, Member S, Ray PK. A new MPPT design using Grey Wolf optimization technique for photovoltaic system under partial shading conditions. IEEE Trans Software Eng 2016;7(1):181–8.
[23] Sharma S, Bhattacharjee S, Bhattacharya A. Grey Wolf optimisation for optimal sizing of battery energy storage device to minimise operation cost of microgrid. IET Gener Transm Distrib 2016;10:625–37. https://doi.org/10.1049/iet-gtd.2015.0429.
[24] Radu-Emil P, Radu-Codrut D, Emil M P. Grey Wolf optimizer algorithm-based tuning of fuzzy control systems with reduced parametric sensitivity. IEEE Trans Ind Electron 2017;64(1):527–34. https://doi.org/10.1109/TIE.2011.2157278.
[25] Luis R, Oscar C, Jos S, Patricia M. A fuzzy hierarchical operator in the Grey Wolf optimizer algorithm. Appl Soft Comput 2017;57:315–28. https://doi.org/10.1016/j.asoc.2017.03.0480.
[26] J. A. Karl, H. Tore, PID controllers: theory, design, and tuning, Instrument Society of America, North Carolina.
[27] W. Liuping, C. Shan, Y. Dae, G. Lu, K. Ng, Electrical drives and power converters using matlab/simulink, Wiley's ebook EULA.
[28] Sonke T, Nils H, Fuchs FW. PI control, PI-based state space control, and model-based predictive control for drive systems with elastically coupled. IEEE Trans Ind Electron 2011;58(8):3647–57. https://doi.org/10.1109/TIE.2014.2354593.
[29] Houari A, Auger F, Olivier J-C, Machmoum M. A new compensation technique for PMSM torque ripple minimization. In: IEEE industry applications society annual MeetingIndustry applications society annual meeting. 2015. p. 1–6.

Please cite this article in press as: Djerioui A, et al. Grey Wolf based control for speed ripple reduction at low speed operation of PMSM drives, ISA Transactions (2018), https://doi.org/10.1109/TIE.2014.2354593